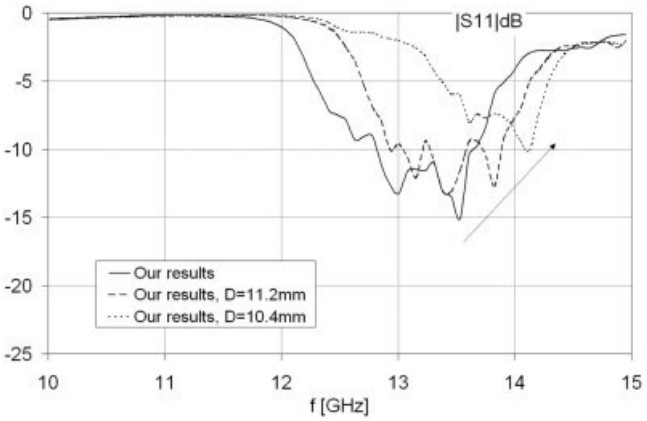

Figure 7 Magnitude of the reflection coefficient S_{11}, as a function of the frequency, for different values of D

trum of the incident field on the EBG coming from the patch radiator, and a subsequent FMM analysis.

REFERENCES

1. K. Yasumoto, Electromagnetic theory and applications for photonic crystals, CRC Press, Boca Raton, FL, 2006.
2. J.D. Joannopoulos, R.D. Meade, and J.N. Winn, Photonic crystals: Molding the flow of light, Princeton University Press, New Jersey, 1995.
3. A.R. Weily, L. Horvath, K.P. Esselle, B.C. Sanders, and T.S. Bird, A planar resonator antenna based on a woodpile EBG material, IEEE Trans Antenn Propag 53 (2005), 216–223.
4. G.S. Smith, M.P. Kesler, and J.G. Maloney, Dipole antennas used with all-dielectric, woodpile photonic-bandgap reflectors: Gain, field patterns, and input impedance, Microwave Opt Technol Lett 21 (1999), 191–196.
5. Y.J. Lee, J. Yeo, R. Mittra, and W.S. Park, Application of electromagnetic bandgap (EBG) superstrates with controllable defects for a class of patch antennas as spatial angular filters, IEEE Trans Antenn Propag 53 (2005), 224–235.
6. I.R. Matias, I.D. Villar, and F.J. Arregui, Comparative study of the modeling of three-dimensional photonic bandgap structures, J Opt Soc Am A 20 (2003), 644–654.
7. L. Li, Fourier modal method for crossed anisotropic gratings with arbitrary permittivity and permeability tensors, J Opt A: Pure Appl Opt 5 (2003), 345–355.
8. L. Li, New formulation of the Fourier modal method for crossed surface-relief gratings, J Opt Soc Am A 14 (1997), 2758–2767.
9. L. Li, Formulation and comparison of two recursive matrix algorithms for modelling layered diffraction gratings, J Opt Soc Am A 13 (1996), 1024–1035.
10. F. Frezza, L. Pajewski, and G. Schettini, Periodic defects in 3D electromagnetic band-gap media, In Proceedings of the 2006 IEEE MTT-S International Microwave Symposium Digest, San Francisco, California, June 11–16, 2006.

© 2006 Wiley Periodicals, Inc.

EXCITATION OF AN ELECTRICALLY SMALL METAMATERIAL-COATED CYLINDER BY AN ARBITRARILY LOCATED LINE SOURCE

Samel Arslanagic,[1] Richard W. Ziolkowski,[2] and Olav Breinbjerg[1]
[1] Ørsted•DTU, Electromagnetic Systems
Technical University of Denmark
Building 348, Ørsteds Plads
DK-2800 Kgs. Lyngby, Denmark
[2] Department of Electrical and Computer Engineering
University of Arizona
1230 E. Speedway Blvd.
Tucson, AZ 85721-0104

Received 15 June 2006

ABSTRACT: *The problem of an arbitrarily located electric line source radiating in the presence of a metamaterial-coated cylinder is solved analytically and implemented numerically. Electrically small resonant metamaterial-coated cylinders are designed that lead to significant enhancements of both the radiated and scattered powers, as compared with the power radiated by the source into free space, as well as the total scattering cross section, as compared with the results obtained for a corresponding cylinder coated with a conventional material. The effects of the dispersion and losses present in the metamaterials are taken into account to study the bandwidth properties of these resonant configurations.* © 2006 Wiley Periodicals, Inc. Microwave Opt Technol Lett 48: 2598–2606, 2006; Published online in Wiley InterScience (www.interscience.wiley.com). DOI 10.1002/mop.21990

Key words: *metamaterial; antenna; scattering; double-negative (DNG) material; single-negative (SNG) material; cylinder*

1. INTRODUCTION

Recently, there has been great interest in exploring and exploiting the electromagnetic characteristics and properties of various classes of metamaterials (MTMs). These MTMs include double-negative (DNG) media, characterized by a negative real part of the permittivity and permeability, first considered by Veselago [1], and single-negative (SNG) media, characterized by a negative real part of either the permittivity (in which case they are referred to as ε-negative (ENG) media) or the permeability (in which case they are referred to as μ-negative (MNG) media). A considerable amount of analysis to understand the properties of both DNG and SNG media has already been performed; see Ref. 2 and the works referenced therein.

The growing interest in MTMs is due to their unusual electromagnetic properties and the potential to exploit them for a variety of applications [1, 2]. Different MTM configurations have been considered, particularly canonical rectangular, cylindrical, and spherical shapes. Among the rectangular geometries, the lossless DNG slab has attracted a great deal of attention due to its so-called "perfect lens" property [3]. Moreover, properties of DNG and SNG mono and bilayers such as resonance, tunneling, and transparency have been investigated as well, e.g., see Ref. 4. The plane wave scattering properties and other interesting features of MTM cylinders and spheres have been investigated in detail in Refs. 2 and 5–19. In particular, it has been demonstrated that electrically small MTM cylindrical as well spherical shells can be designed to produce resonant source and scattering configurations [2, 8, 9, 16–18] leading to significant enhancements of the total radiated and scattered powers, as well as the total scattering cross section.

The purpose of the present work is to design electrically small resonant MTM-coated cylinders in the presence of an arbitrarily

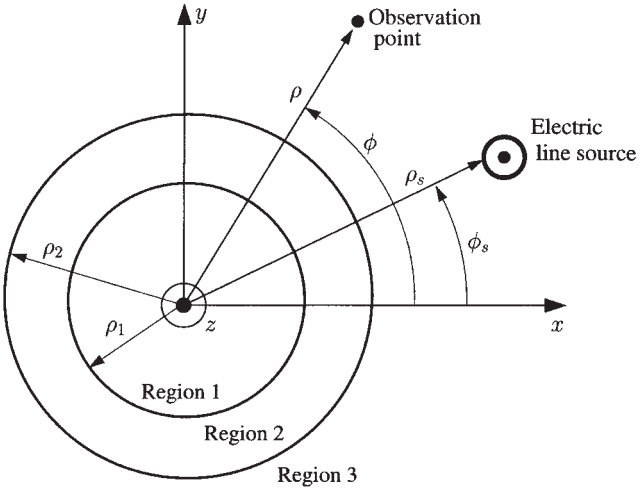

Figure 1 The electric line source excited MTM-coated cylinder configuration

located infinite electric line source (ELS),[1] and to show that these likewise lead to enhancements of the radiated and scattered powers, as compared with the power radiated by the source into free space, as well as the total scattering cross section, as compared with the results obtained for a corresponding cylinder coated with a conventional material. The present manuscript is organized as follows. In Section 2, the analytical solution to the problem at hand is derived and the terms used to quantify the results are defined. In Section 3, the conditions for resonance are derived and results are shown for specifically designed electrically small structures. The important differences between electrically small two-dimensional (2D) and three-dimensional (3D) structures are emphasized and negative conclusions reached in Ref. 19, regarding the possibility of achieving resonant cylindrical structures, are discussed. The effects of dispersion are taken into account in Section 4 to study the bandwidth properties of the resonant configurations identified in Section 3. Furthermore, the fundamental distinctions between the present structures and those for which the resonant behavior is related to the overall size of the structure are pointed out in Section 5. Throughout the manuscript, the time factor $\exp(j\omega t)$, with ω being the angular frequency and t being the time, is assumed and suppressed.

2. ANALYTICAL SOLUTION

The configuration of interest is depicted in Figure 1. It represents a concentric pair of infinite circular cylinders consisting of a central core (Region 1) covered with one layer of MTM (Region 2), both of which can be composed of a simple double-positive (DPS) material characterized by a positive real part of both the permittivity and permeability, as well as DNG or SNG materials. The exterior region, Region 3, is free space with the intrinsic impedance denoted by η_3. The MTM-coated cylinder is illuminated by an infinite ELS with a constant electric current I_e [A]. The axes of the cylinders and the ELS are parallel, and the ELS can be located in any of the three regions. Region i, with $i = 1, 2, 3$, is characterized by a permittivity and a permeability, denoted by ε_i and μ_i, respectively, while the wave number inside Region i is denoted by k_i and given by $k_i = \omega\sqrt{\varepsilon_i}\sqrt{\mu_i}$, where the branch of the square root is chosen so that $\mathrm{Im}\{k_i\} \leq 0$. A cylindrical coordinate system (ρ,φ,z) and the associated Cartesian coordinate system (x,y,z) are introduced such that the z-axis coincides with the axes of the cylinders. The coordinates of the observation point are (ρ,φ), while the coordinates of the ELS are (ρ_s,φ_s).

Using the cylindrical wave functions that originate at $\rho = 0$, the incident electric field generated by the ELS is given by the well-known expression [20]

$$\vec{E}_{\mathrm{ELS}}(\rho,\varphi) = -\hat{z}I_e\frac{\omega\mu_{\mathrm{ELS}}}{4}\begin{cases}\sum_{n=0}^{N_{\max}}\varepsilon_n J_n(k_{\mathrm{ELS}}\rho)H_n^{(2)}(k_{\mathrm{ELS}}\rho_s)\cos[n(\varphi-\varphi_s)] & \text{for } \rho \leq \rho_s,\\ \sum_{n=0}^{N_{\max}}\varepsilon_n J_n(k_{\mathrm{ELS}}\rho_s)H_n^{(2)}(k_{\mathrm{ELS}}\rho)\cos[n(\varphi-\varphi_s)] & \text{for } \rho \geq \rho_s,\end{cases} \quad (1)$$

where $J_n(\cdot)$ is the Bessel function of order n and is chosen to represent the field for $\rho \leq \rho_s$ due to its nonsingular behavior at the origin, while $H_n^{(2)}(\cdot)$ is the Hankel function of second kind and order n, and is chosen for $\rho \geq \rho_s$ because it represents an outward propagating wave that complies with the radiation condition. In addition, μ_{ELS} and k_{ELS} are, respectively, the permeability and wave number of the medium in which the ELS is located. The symbol ε_n is the Neumann number; thus $\varepsilon_n = 1$ for $n = 0$, and $\varepsilon_n = 2$ otherwise. Furthermore, $N_{\max}$ is the truncation limit and is chosen in a manner that ensures convergence.

The scattered fields in each of the regions are likewise expanded in terms of cylindrical wave functions, and are given by

$$\vec{E}_{1s}(\rho,\varphi) = -\hat{z}I_e\frac{\omega\mu_1}{4}\sum_{n=0}^{N_{\max}}\varepsilon_n C_{1n}J_n(k_1\rho)\cos[n(\varphi-\varphi_s)] \text{ for } \rho \leq \rho_1, \quad (2a)$$

$$\vec{E}_{2s}(\rho,\varphi) = -\hat{z}I_e\frac{\omega\mu_2}{4}\sum_{n=0}^{N_{\max}}\varepsilon_n[C_{2n}J_n(k_2\rho) + C_{3n}Y_n(k_2\rho)]\cos[n(\varphi-\varphi_s)] \text{ for } \rho_1 \leq \rho \leq \rho_2, \quad (2b)$$

$$\vec{E}_{3s}(\rho,\varphi) = -\hat{z}I_e\frac{\omega\mu_3}{4}\sum_{n=0}^{N_{\max}}\varepsilon_n C_{4n}H_n^{(2)}(k_3\rho)\cos[n(\varphi-\varphi_s)] \text{ for } \rho \geq \rho_2, \quad (2c)$$

where $C_{in}, i = 1,\ldots,4$ are the unknown scattered field expansion coefficients and $Y_n(\cdot)$ is the Neumann function of order n. The corresponding incident and scattered magnetic fields, which are required in the determination of the unknown expansion coefficients, are readily obtained from Faraday's law. Enforcing the electromagnetic field boundary conditions at the interfaces $\rho = \rho_1$ and $\rho = \rho_2$, respectively, it is easily shown that the unknown expansion coefficients are found from the following relation.

$$\vec{C}_n = \overline{\overline{\mathrm{M}}}_n^{-1}\vec{\Lambda}_n, \quad n = 0,1,2,\ldots,N_{\max}, \quad (3)$$

where $\vec{C}_n = [C_{1n.}C_{2n.},C_{3n.},C_{4n.}]$ is the vector containing the four unknown coefficients, $\Lambda_n = [\Lambda_{1n.}\Lambda_{2n.},\Lambda_{3n.},\Lambda_{4n.}]$ is the excitation vector and this is different for different locations of the ELS. The elements of this vector when the ELS is located in Regions 1, 2, and 3, respectively, are shown in Table 1.

[1]The ELS type of illumination corresponds to TM polarization. The results for the magnetic line source illumination, which correspond to TE polarization, are easily obtained by duality and are not included here.

The matrix $\overline{\overline{\mathrm{M}}}_n$ is a four-by-four matrix that contains the remaining terms associated only with the scattered field components and is given by

$$\overline{\overline{\mathrm{M}}}_n = \begin{bmatrix} -\mu_1 J_n(k_1\rho_1) & \mu_2 J_n(k_2\rho_1) & \mu_2 Y_n(k_2\rho_1) & 0 \\ -k_1 J_n'(k_1\rho_1) & k_2 J_n'(k_2\rho_1) & k_2 Y_n'(k_2\rho_1) & 0 \\ 0 & \mu_2 J_n(k_2\rho_2) & \mu_2 Y_n(k_2\rho_2) & -\mu_3 H_n^{(2)}(k_3\rho_2) \\ 0 & k_2 J_n'(k_2\rho_2) & k_2 Y_n'(k_2\rho_2) & -k_3 H_n^{(2)\prime}(k_3\rho_2) \end{bmatrix}. \tag{4}$$

In the above expressions, the prime denotes the derivative with respect to the argument, i.e., $B_n'(x) = \mathrm{d}B_n(x)/dx$, where $B_n(x)$ represents any of the involved cylindrical wave functions.

The figures of merit to be investigated in this manuscript are the total radiated (or scattered)[2] power and the total scattering cross section. Since the configuration at hand is infinite in the z-direction, all of the quantities are determined on a *per unit length* basis. The total power can be expressed as

$$P_{\mathrm{t}} = \lim_{\rho\to\infty} \frac{1}{2\eta_3} \int_{\varphi=0}^{2\pi} |\vec{E}_{\mathrm{t}}(\rho,\varphi)|^2 \, \rho d\varphi = \left(\frac{1}{4}\eta_3 I_e^2\right) \times \left[\frac{k_3}{4} \sum_{n=0}^{N_{\max}} \varepsilon_n^2 (3-\varepsilon_n) |\alpha_n|^2\right], \tag{5}$$

where $\vec{E}_{\mathrm{t}}$ denotes the total field in Region 3, while $\alpha_n = C_{4n}$ when the ELS is in either Region 1 or 2, and $\alpha_n = J_n(k_3\rho_s) + C_{4n}$ when the ELS is in Region 3. The power radiated by the ELS alone in free space, denoted by P_i, is given by Eq. (6) with α_n replaced by $J_n(k_3\rho_s)$. More specifically,

$$P_i = \left(\frac{1}{4}\,\eta_3 I_e^2\right)\left[\frac{k_3}{4} \sum_{n=0}^{N_{\max}} \varepsilon_n^2 (3-\varepsilon_n) |J_n(k_3\rho_s)|^2\right] = \left(\frac{1}{4}\,\eta_3 I_e^2\right)\left[\frac{k_3}{2}\right], \tag{6}$$

where the sum has been evaluated using the well-known result in Ref. 21. Of particular interest to the present manuscript is the comparison of the total power in the presence of the MTM-coated cylinder with that radiated by the ELS alone. To this end, the quantity designated the power ratio (PR)[3], and denoted by P_{r}, is introduced and this is given by

$$P_{\mathrm{r}} = \frac{P_{\mathrm{t}}}{P_i} = \frac{1}{2} \sum_{n=0}^{N_{\max}} \varepsilon_n^2 (3-\varepsilon_n) |\alpha_n|^2. \tag{7}$$

The total scattering cross section, denoted by σ_{t}, used when the ELS is in Region 3, is defined by the ratio of the power contained in the scattered far-field to the incident power density at the origin, and is given by

[2]The term total radiated power applies for the configurations where the ELS is located in Regions 1 and 2, while the term total scattered power is used in the case where the ELS is located in Region 3. Henceforth, only the term total power is used, since it will be clear from the context of its usage which power is actually being referred to.

[3]In similitude with the power terms, the PR is understood as the radiated PR when the ELS is in Regions 1 and 2, while it is understood as the scattered PR when the ELS is in Region 3.

TABLE 1 The Elements Λ_{in}, i = 1, 2, 3, and 4, of the Excitation Vector $\vec{\Lambda}_n$ When the ELS is Located in regions 1, 2, or 3, Respectively

	ELS		
Λ_{in}	Region 1	Region 2	Region 3
Λ_{1n}	$\mu_1 J_n(k_1\rho_s) H_n^{(2)}(k_1\rho_1)$	$-\mu_2 J_n(k_2\rho_1) H_n^{(2)}(k_2\rho_s)$	0
Λ_{2n}	$k_1 J_n(k_l\rho_s) H_n^{(2)},(k_1\rho_1)$	$-k_2 J(k_2\rho_1) H_n^{(2)}(k_2\rho_s)$	0
Λ_{3n}	0	$-\mu_2 J_n(k_2\rho_s) H_n^{(2)}(k_2\rho_2)$	$\mu_3 J_n(k_3\rho_2) H_n^{(2)}(k_3\rho_s)$
Λ_{4n}	0	$-k_2 J_n(k_2\rho_s) H_n^{(2)}(k_2\rho_2)$	$k_3 J_n'(k_3\rho_2) H_n^{(2)}(k_3\rho_s)$

$$\sigma_{\mathrm{t}} = \frac{\lim\limits_{\rho\to\infty} \int_{\varphi=0}^{2\pi} |\vec{E}_{3s}(\rho,\varphi)|^2 \rho \, d\varphi}{|\vec{E}_{\mathrm{ELS}}(0,0)|^2} = \frac{2}{k_3} \frac{\sum_{n=0}^{N_{\max}} \varepsilon_n^2 (3-\varepsilon_n) |C_{4n}|^2}{|H_0^{(2)}(k_3\rho_s)|^2}. \tag{8}$$

In the following section, numerical results for the power ratio and the total cross section, obtained for electrically small MTM-coated cylinders in the presence of an arbitrarily located ELS, are presented and discussed. Throughout the following assessments, a structure in which Regions 1 and 2 are both composed of a DPS material is referred to as a DPS-DPS structure, while it is referred to as a DPS-DNG structure if one of the regions consists of a DNG material.

3. NUMERICAL RESULTS

To provide more insight into the physics associated with the electrically small cylindrical structures, it is useful to find the conditions for which the enhancements of the total power and total scattering cross section will occur. Since in the general case both the total power (Eq. (5)) and the total scattering cross section (Eq. (8)) are proportional to $|C_{4n}|^2$, large values for these quantities will result if the amplitude of the scattering coefficient C_{4n} is correspondingly large. Such large values of the scattering coefficients are related to the presence of the so-called natural modes (also known as material polaritons), and the corresponding peaks in the scattering coefficients are referred to as natural resonances, see e.g., Refs. 8–10 and the works referenced therein. When the structure of interest (be it antenna-like or cavity-like structure) is made of DPS materials, it is well known that the natural resonances occur only if the size of the structures is on the order of, or larger than, the wavelength inside the material. These wavelength-sized natural resonances will be discussed briefly in Section 5. However, when the structure is formed by combinations of DPS, DNG, and/or SNG materials, the scattering coefficients may exhibit peaks (and thus resonances) even if the structures are significantly smaller than the wavelength [8–10]. As explained in Refs. 8–10, these resonances are attributed to the clever pairing of DPS, DNG, and/or SNG materials, and are referred to as interface resonances in Refs. 8 and 9. To find the condition for which the amplitudes of the scattering coefficients (and thus of the C_{4n}) become large, one first notes that according to Eq. (3), the scattering coefficients C_{in} are proportional to the product of the inverse of the matrix $\overline{\overline{\mathrm{M}}}_n$ and the excitation vector $\overline{\Lambda}_n$. Since the inverse of a matrix is inversely proportional to the determinant of the matrix, it follows that C_{in} are proportional to the inverse of the determinant of $\overline{\overline{\mathrm{M}}}_n$. When the magnitude of this determinant attains a minimum, the amplitude of C_{in} becomes very large, and resonance occurs, thus leading to enhancements of the total power and total scattering cross section. Since the structures to be emphasized here are

TABLE 2 Material and Geometrical Parameters for the Very Electrically Small Dipolar and Quadrupolar Resonant Configurations

Structure	ε_2	μ_2	ρ_1 (mm)	ρ_2 (mm)
Dipolar	$\pm\varepsilon_0$	$\pm 4\mu_0$	6	10
Quadrupolar	$\pm\varepsilon_0$	$\pm 4\mu_0$	3.8729	5

electrically small, the small argument expansions of the functions contained in $\overline{\overline{M}}_n$ are used to derive an approximate analytical expression for the resonance condition. For the range of parameters to be investigated here, it can be shown that the C_{in} exhibit a resonance when the approximate condition

$$\frac{\rho_1}{\rho_2} \approx 2n \sqrt{\frac{(\mu_2 + \mu_1)(\mu_2 + \mu_3)}{(\mu_2 - \mu_1)(\mu_2 - \mu_3)}}, \quad n \geq 1 \tag{9}$$

is met. This condition is used here to determine, for a given set of material parameters, the approximate ratio of ρ_1 and ρ_2 that yields a resonant MTM-coated cylinder. The condition for the electrically small resonant structure given by Eq. (9) depends on the mode number, n, a careful choice of material parameters, and only on the ratio of the inner and outer radii of Region 2, and thus not on how small either of these radii are individually. It is worth emphasizing that Eq. (9) holds for $n \geq 1$, and that for the range of parameters to be investigated here, the $n = 0$ (i.e., the monopolar) mode does not show a similar resonant behavior. This implies that there is no electrically small monopolar structure that will have a resonance. Relation (9) is identical to the one obtained in Refs. 8 and 9 for plane wave scattering from the cylindrical structures considered here. Though certain small terms have been neglected in the derivation of Eq. (9), this condition constitutes a very accurate approximation for the radii ratio as will be shown in the following. Hence, Expression (9) also merely serves as a guideline to estimate the resonant configuration, i.e., as a starting point for the numerical analysis. In particular, since the numerical solution is implemented without the use of any small argument expansions, the results will be exact. The values of ρ_1 and ρ_2 so obtained will be the ones used to define the resonant structures associated with the total power and total cross-section investigations. We also note that Eq. (9) can be satisfied only for specific combinations of MTM coatings. One observes that for the TM polarization investigated here, the resonance condition can be met with either DPS-DNG or DPS-MNG structures, since Eq. (9) is independent of the permittivity of the different regions. The DPS-DNG structures are emphasized in the discussion below.

Having clarified the condition for a resonance to occur, an interesting observation for the configurations in which the ELS is located in Region 1 along the axis of the cylinders, i.e., for $\rho_s = 0$, is made. From Table 1 it is understood that the nonzero elements of the excitation vector $\overline{\Lambda}_n$ for the ELS in Region 1 are proportional to $J_n(k_1\rho_s)$. Since $J_n(0) = 0$ for $n > 0$, only the monopolar mode radiates when the ELS is located on the axis of the cylinders. Since there is no electrically small monopolar resonant structure for the range of parameters to be investigated here, one concludes that the resonances associated with the electrically small MTM-coated cylinders occur only for $n = 1$ (dipolar), $n = 2$ (quadrupolar), and higher-order modes when the ELS is located off the cylinder axis, i.e., for $\rho_s > 0$ and for $n \geq 1$[4]. These observations highlight one of the most important differences between the electrically small 2D and 3D structures, and have an immediate impact on some results reported in the literature, in particular the negative conclusions reached in Ref. 19 about achieving the very electrically small resonant configurations. In sharp contrast to the $\rho_s = 0$ case, the $\rho_s > 0$ 2D configurations do show the resonant behaviors expected from the 3D cases. Their presence in several DPS-DNG structures and their absence in the corresponding DPS-DPS cases will be demonstrated below. Furthermore, as reported, for instance, in Refs. 7and 13, it is also demonstrated (see Section 5) that larger cylindrical structures will exhibit resonances for both the DPS-DPS and DPS-DNG cases when the ELS is located at the center of the cylinders where $\rho_s = 0$.

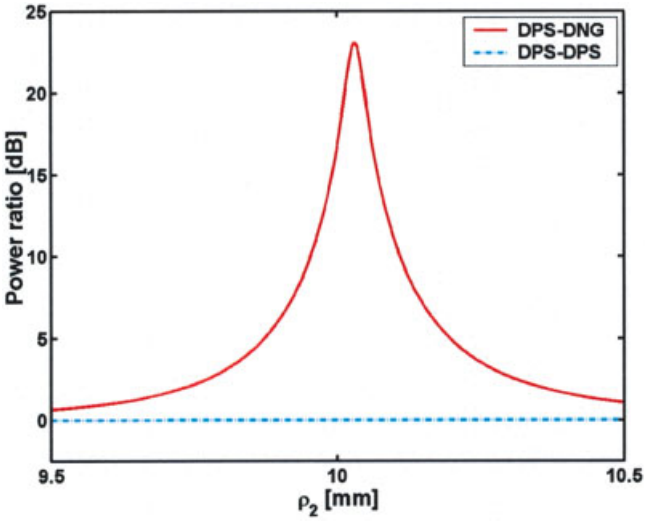

Figure 2 PR as a function of the outer shell radius ρ_2 for the DPS-DNG and DPS-DPS dipolar structures when the ELS is in Region 1 at $\rho_s = 5.99$ mm. [Color figure can be viewed in the online issue, which is available at www.interscience.wiley.com]

In Table 2, the parameters that define several very electrically small resonant structures are summarized. Regions 1 and 3 were assumed to be free space, while Region 2 was taken to be a specified DNG medium. The radius ratio (Eq. (9)) for these fixed material parameters was obtained for the dipolar and quadrupolar modes. The outer radius was selected and the inner radius reported in Table 2 was obtained from this ratio. The positive material parameters in Region 2 of the corresponding reference DPS-DPS structures are also indicated in Table 2. Throughout this discussion, the frequency of operation, denoted by f_0, is 300 MHz implying that the free-space wavelength, denoted by λ_0, is 1 m.

From both Relation (9) and Table 2, it follows that for fixed material parameters, a considerably thinner structure is needed to excite the quadrupolar mode than the dipolar mode. The resonant dipolar mode excited in the DPS-DNG structure is illustrated first. Figure 2 shows the PR, as a function of the outer radius ρ_2, when the inner radius is fixed at $\rho_1 = 6$ mm for the DPS-DNG and DPS-DPS structures. The ELS is located in Region 1 at $\rho_s = 5.99$ mm. The ELS location is chosen near the interface of the DPS and DNG layers because it produces the largest peak PR

[4]In relation to this, it is interesting to note that the higher-order modes are also responsible for the resonant effects associated with the very electrically small 3D dipole-spherical MTM structures treated in Refs. 10, 16–18. This statement encompasses even the reciprocity behavior identified in Ref. 10.

values for the outer radius scans for DPS-DNG structures. For the DPS-DNG structure, a resonance peak (of value $PR \approx 23dB$ or $PR \approx 200$) is found in the PR values at $\rho_2 = 10.03$ mm, which is very close to the approximate value of 10 mm obtained from Eq. (9). The PR values for the corresponding DPS-DPS structure are also given in Figure 2. In distinct contrast to the DPS-DNG structure, no resonances and hence enhancements of the total power are observed for this DPS-DPS structure. For the DPS-DPS case the peak $PR \approx 0.01dB$, i.e., it is very close to unity.

The electric near-field distribution[5] of the resonant dipolar mode excited in the DPS-DNG structure for which $\rho_2 = 10.03$ mm when the ELS is located at $\rho_1 = 5.99$ mm is illustrated in Figure 3(a). Similar results, not included here, have been obtained for dipolar DPS-DNG and DPS-DPS structures for which the ELS is located in Regions 2 and 3.

To demonstrate the influence of the ELS location on the resonant enhancements of the total power, Figures 4(a), 3(b), and 3(c) show, respectively, the PR as a function of the ELS position, ρ_s, with the ELS in regions 1, 2, and 3 for the DPS-DNG and DPS-DPS structures having the fixed radii: $\rho_1 = 6$ mm and $\rho_2 = 10.03$ mm. In particular, the ELS location varies in the interval $\rho_s \in [1\text{–}5.99]$ mm in Figure 4(a), in $\rho_s \in [6.01\text{–}9.99]$ mm for Figure 4(b), and in $\rho_s \in [10.1\text{–}25]$ mm for Figure 4(c). In all cases and regardless of the location of the ELS, the DPS-DPS structures offer no enhancement, i.e., the maximum PR value is very close to unity: $PR \approx 0.01\ dB$. In contrast, the corresponding DPS-DNG structures offer very large values for the PR, this being particularly true when the ELS is nearby the interfaces of the DPS and DNG layers. As the ELS is moved through Region 1, the PR increases from values near zero to ~23 dB, when the ELS is near the inner surface of the first cylinder. The demonstrated fact that there is no enhancement when the ELS is near the origin confirms the previously stated fact that the ELS must be offset from the origin to excite, in this case, the resonant dipolar mode.

With regards to the ELS in Region 2, the largest PR values are obtained for the ELS near the interfaces of the DPS and DNG layers. However, the behavior of the PR as a function of ρ_s, when the ELS is in Region 2, is particularly interesting because it exhibits a minimum for a particular ELS position. This minimum occurs at $\rho_s = 7.746076$ mm; the total power radiated by the ELS in the presence of the DNG coating is actually slightly lower than the power radiated by the ELS alone. It is found that as the ELS is moved in the DNG region, its ability to excite the resonant dipolar mode changes. In particular, for the minimum PR location value, it is found that the ELS couples only to the monopolar mode. Since the ELS cannot couple to the dipolar mode, as is the case when it is located at the origin, it cannot cause a resonant enhancement of the total power. In addition to these findings, it is interesting to note that the PR is considerably less sensitive with respect to the position of the ELS than it is to the outer radius of the MTM coating.

When the ELS is located in Region 3, it is of further interest to investigate the behavior of the total scattering cross section σ_t; i.e., while the ELS and the MTM-coated cylinder can be considered as a radiating system when the ELS is in Regions 1 and 2, the MTM-coated cylinder can be considered as a scatterer excited by the ELS when it is in Region 3. Figure 5(a) shows σ_t as a function of the outer radius ρ_2 when the inner radius $\rho_1 = 6.0$ mm, and the source is located at $\rho_2 = 10.51$ mm. Results for both the DPS-DNG and DPS-DPS structures are shown. As observed in Figure 5(a), the cross section is enhanced considerably by the presence of the DNG coating when $\rho_2 = 10.03$ mm, even though the structure is electrically small. Thus, as shown in Ref. 10, for the correspond-

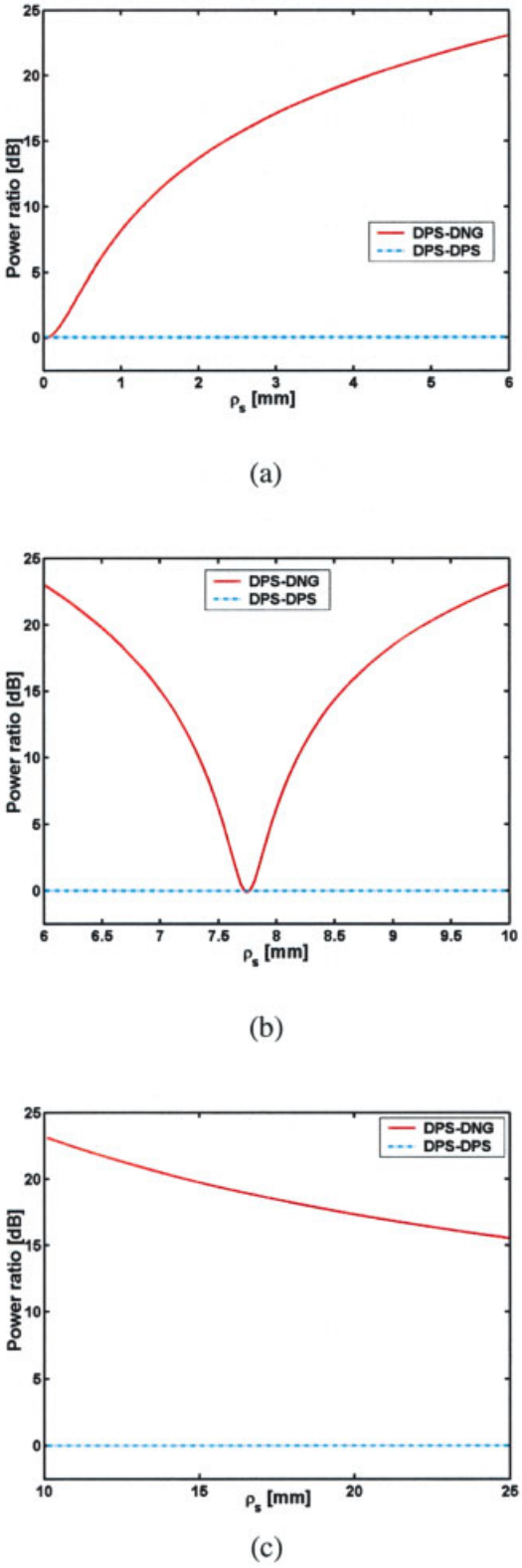

Figure 3 Electric near-field distribution for the resonant dipolar (a) and quadrupolar (b) DPS-DNG structures. [Color figure can be viewed in the online issue, which is available at www.interscience.wiley.com]

[5]In Figure 5, the total electric near-field, denoted by $\tilde{E}(\rho,\varphi)$, or more specifically, the quantity $20\log_{10}|E(\rho,\varphi)|$, where $\tilde{E}(\rho,\varphi)$ has been normalized by IV/m prior to taking the logarithm, is shown in a circular region of radius $3\rho_2$ centered at the cylinder axis (z-axis) (see Figure 1).

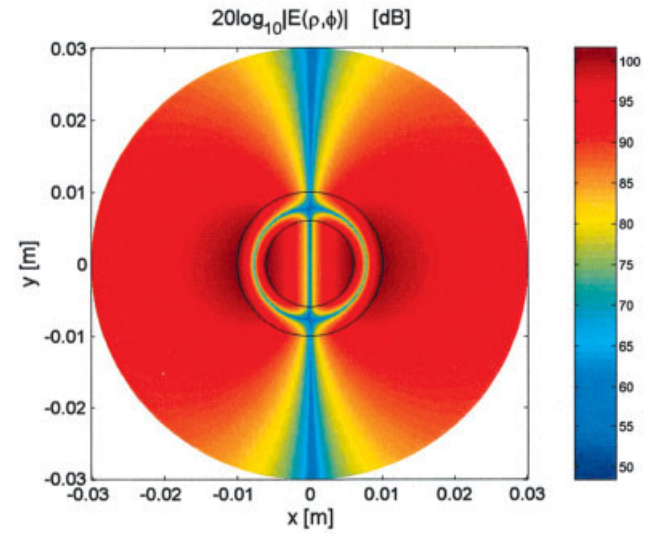

(a)

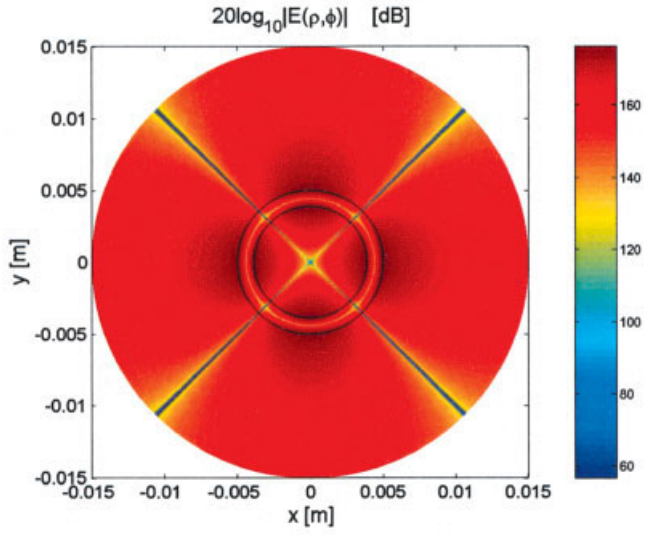

(b)

Figure 4 PR as a function of the ELS location ρ_s for the DPS-DNG and DPS-DPS dipolar structures when the ELS is in Region 1 (a), Region 2 (b), and Region 3 (c)

ing sphere case, the present radiating and scattering systems are reciprocal. Furthermore, Figure 5(b) depicts the total cross section as a function of the ELS location, ρ_s. In analogy to the total power, the largest total cross-section values occur when the ELS is placed near to the outer surface of the DNG coating.

Equation (9) indicates that resonant enhancements for particular DPS-DNG structures can also occur for the quadrupolar mode, while again none are possible for the corresponding DPS-DPS cases. Figure 6(a) shows the PR as a function of the outer radius ρ_2 for DPS-DNG and DPS-DPS structures that have ρ_1 = 3.8729 mm and the permittivity and permeability values in Region 2 given in Table 2. The ELS is located in Region 1 at ρ_s = 3.8 mm. As with the dipolar mode, the location of the ELS near the DPS-DNG interface is presented because it produces the largest enhancements for the DPS-DNG structures. Resonance, and thus the enhancement of the total power, is indeed observed in Figure 6(a) for the DPS-DNG structure, with the maximum obtainable PR being approximately: PR $\approx$ 55 dB (or PR $\approx 3.65\times10^5$) when ρ_2=5.000068 mm. This exact value is very close to the approximate value of 5 mm listed in Table 2. In comparison to the dipolar case, the enhancements for the quadrupolar case are significantly larger, but the resonance is proportionally extremely narrow and extremely sensitive to even very slight changes in the material and/or geometrical parameters or the frequency of operation. Figure 6(a) also shows that no enhancements of the total

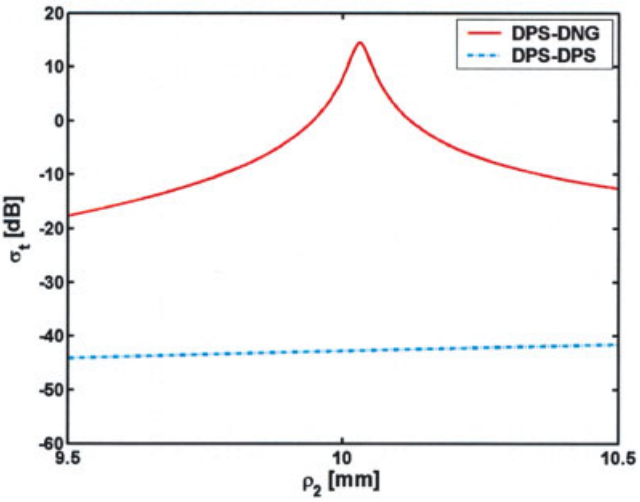

(a)

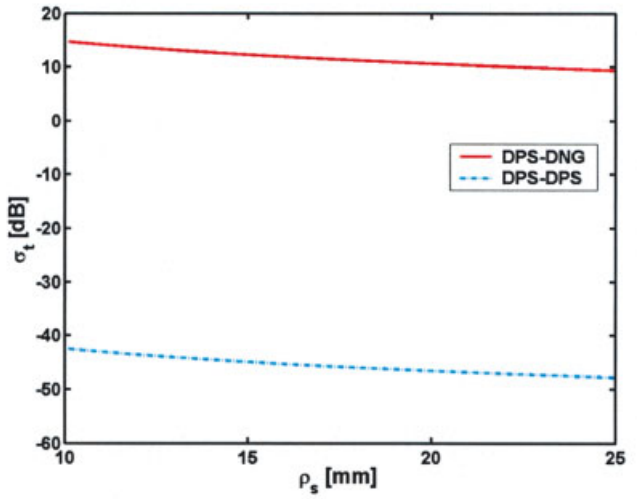

(b)

Figure 5 The total scattering cross section σ_t as a function of the outer shell radius ρ_2 (a) and the ELS location ρ_s (b) for the DPS-DNG and DPS-DPS dipolar structures. [Color figure can be viewed in the online issue, which is available at www.interscience.wiley.com]

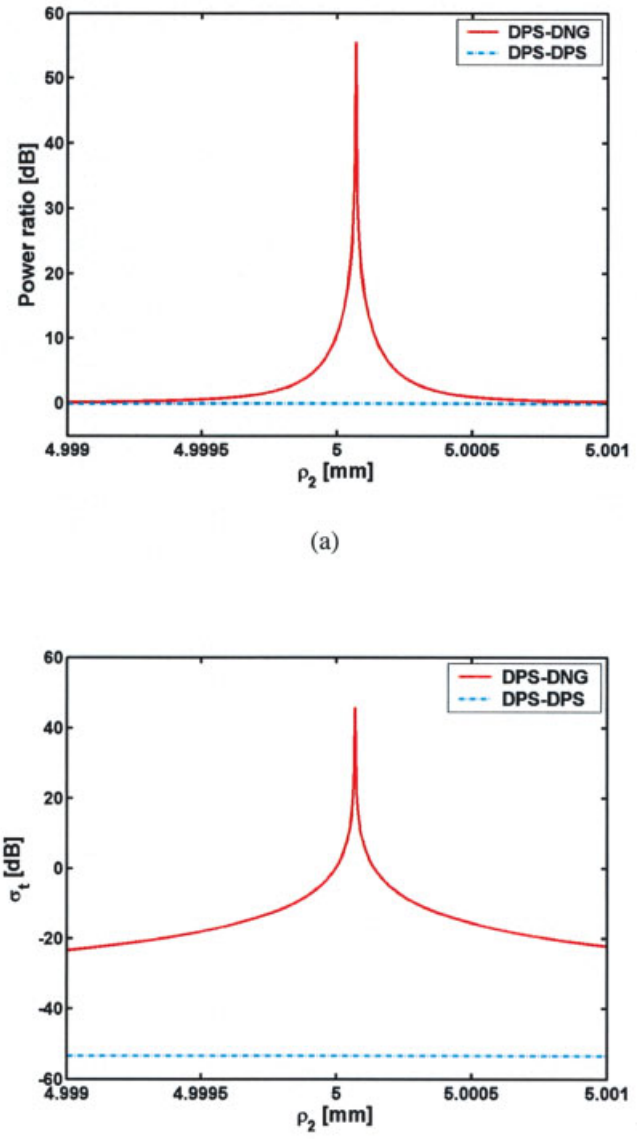

Figure 6 PR when the ELS is in Region 1 at $\rho_s = 3.8$ mm (a) and the total scattering cross section σ_t (b) as a function of the outer shell radius ρ_2 for the DPS-DNG and DPS-DPS quadrupolar structures. [Color figure can be viewed in the online issue, which is available at www.interscience.wiley.com]

power are obtained for the corresponding DPS-DPS structure. The electric near-field distribution for the resonant quadrupolar mode excited in the DPS-DNG structure for which $\rho_2 = 5.000068$ mm when the ELS is located at $\rho_s = 3.8$ mm is illustrated in Figure 3(b). Similar results, not included here, have been obtained for quadrupolar DPS-DNG and DPS-DPS structures for which the ELS is located in Regions 2 and 3.

For the case of the ELS in Region 3, the total scattering cross section for the quadrupolar structure for which the ELS is at $\rho_s = 5.1$ mm is shown in Figure 6(b). A resonant enhancement is observed at $\rho_2 = 5.000068$ mm, while no enhancement is found for the corresponding DPS-DPS structure.

4. EFFECTS OF DISPERSION AND LOSSES

To assess the effects of dispersion and losses on the resonant behavior of the DPS-DNG structures, the well-known Drude and Lorentz models of both the permittivity and permeability were used. The lossy Drude model of the permittivity and permeability, respectively, read

$$\varepsilon_2(\omega) = \varepsilon_0\left(1 - \frac{\omega_{pe}^2}{\omega(\omega - j\Gamma_e)}\right), \tag{10a}$$

$$\mu_2(\omega) = \mu_0\left(1 - \frac{\omega_{pm}^2}{\omega(\omega - j\Gamma_m)}\right), \tag{10b}$$

and the lossy Lorentz model of the permittivity and permeability, respectively, read

$$\varepsilon_2(\omega) = \varepsilon_0\left(1 - \frac{\omega_{pe}^2}{\omega^2 - j\Gamma_e\omega - \omega_{er}^2}\right), \tag{11a}$$

$$\mu_2(\omega) = \mu_0\left(1 - \frac{\omega_{pm}^2}{\omega^2 - j\Gamma_m\omega - \omega_{mr}^2}\right). \tag{11b}$$

In the above relations ω_{pe} and ω_{pm} are the electric and magnetic plasma frequencies, while Γ_e and Γ_m are the electric and magnetic collision frequencies. In the Lorentz models, ω_{er} and ω_{mr} are the resonance frequencies of the permittivity and permeability, respectively.

These models were designed to recover at the angular frequency of operation, $\omega_0 = 2\pi f_0$, where $f_0 = 300$ MHz, the values of the lossless permittivity and permeability given in Table 2, which were used in the cases discussed above. For both models, the assumption $\Gamma_e = \Gamma_m = \xi_e\omega_0 = \xi_m\omega_0 = \xi\omega_0$ with $\xi = 10^{-5}$ was made. This choice means that the losses are very small but are not negligible. For the Drude models, the values of ω_{pe}^2 and ω_{pm}^2 are determined from the real part of Eqs. (10a) and (10b), respectively, evaluated at ω_0 to recover the desired material parameter values. For the Lorentz models, with the assumption that the losses are small, the frequency of operation f_0 must lie above the resonance frequency to obtain the required negative values of the material parameters. Since the angular frequencies of the permittivity and permeability at resonance are given by $\omega_{er} = 2\pi f_{er} = \omega_{mr} = 2\pi f_{mr} = 2\pi f_r$, we set $f_r = 290$ MHz and then determined the values of ω_{pe}^2 and ω_{pm}^2 for the Lorentz models from the desired values of the real parts of Eqs. (11a) and (11b).

The effects of dispersion and losses on the performance of the electrically small dipolar DPS-DNG structures examined above are shown in Figure 7. The PR values for the structures involving the nondispersive DNG coating and the dispersive Drude and Lorentz DNG coatings, respectively, are given for the same dipolar resonant configurations considered in Figure 2. The general characteristics of the results are that the PR is almost constant in the depicted frequency range when the DNG coating is nondispersive; hence, these structures are rather broad band. On the other hand, the results show clearly that when the DNG coating is dispersive, the bandwidth of the resonance attained at $f_0 = 300$ MHz is narrowed considerably when either of the two dispersion models is introduced. The Lorentz model results clearly have a much narrower bandwidth than those obtained with the Drude model. It is also interesting to note that the maximum of the PR obtained with either dispersion model is only slightly lower than the one obtained for the nondispersive case. Again, this decrease is the most profound for the Lorentz dispersion model. This behavior is expected

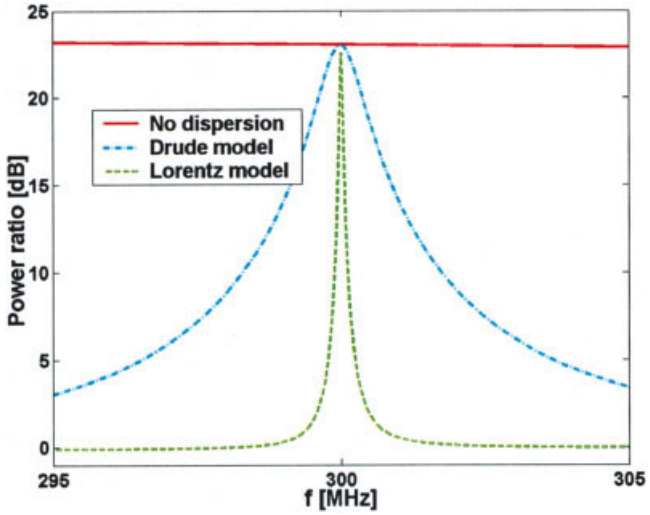

Figure 7 PR as a function of the frequency for the DPS-DNG cases in which the DNG coating is described by a nondispersive model and by Drude and Lorentz dispersion models. The ELS is in Region 1. [Color figure can be viewed in the online issue, which is available at www.interscience.wiley.com]

because of the losses present in both dispersion models, the loss being more severe in the Lorentz model case because the frequency of operation is near the resonance frequency of the material parameters. At $f_0 = 300$ MHz, the PR value in the nondispersive case is 23.05 dB, while it is 23.02 dB for the Drude dispersion model, and 22.56 dB for the Lorentz dispersion model. Similar results, not included here, have been obtained for dipolar DPS-DNG structures for which the ELS is located in Regions 2 and 3.

Note that only the results for the dipolar DPS-DNG structures have been presented. It must be stressed that similar features and comparisons occur when the quadrupolar and higher-order DPS-DNG structures are considered. However, these structures have significantly narrower bandwidths and are, therefore, more easily affected by the presence of dispersion and losses than the dipolar mode. Because the bandwidths of these quadrupolar features are extremely difficult to resolve when the frequency of operation is $f_0 = 300$ MHz, they have not been included here.

5. WAVELENGTH-SIZED NATURAL RESONANCES

It was noted above that very electrically small MTM-coated cylinders with the ELS located exactly at the origin cannot lead to total power enhancements because the ELS is only able to excite the monopolar mode and none of the higher-order modes that are required for these enhancements. Nonetheless, it is important to mention that with sufficiently large DPS and DNG-based structures, the so-called natural resonances of those structures can be excited. They occur when the physical size of the object is related to multiples of the wavelength [8, 9]. To illustrate this point, it is sufficient to treat DPS-DPS and DPS-DNG structures having the same material parameters given in Table 2. As above, the frequency of operation is $f_0 = 300$ MHz; and the ELS is located at the origin, i.e., $\rho_s = 0$ mm. The inner radius of Region 2 is fixed at $\rho_1 = 10$ mm, and the outer one is allowed to vary in the interval $\rho_2 \varepsilon [10,300]$ mm. Figure 8 shows the behavior of the PR as a function of ρ_2. Clearly, both the DPS-DPS and DPS-DNG structures exhibit resonances even though the ELS is on the axis. For the DPS-DPS structure the resonance is attained at $\rho_2 = 178.49$ mm and at $\rho_2 = 208.36$ mm for the DPS-DNG structure. The maximum value is PR=9.59 dB for the DPS-DPS structure, and for the DPS-DNG structure it is PR=9.72 dB. These results show that when the size of the cylinders is in the natural resonance regime, the DPS-DNG structures do not offer any advantage over the corresponding DPS-DPS structures. This is in agreement with the results given in Refs. 7 and 13. This holds in fact for all locations of the ELS. This is in sharp contrast to the very electrically small MTM structures treated in Section 3, where the interface resonances led to the extremely large enhancements.

The wavelength-sized natural resonance phenomenon is familiar from wave guide and cavity theory. It is recalled that a natural mode of a cylindrical wave guide or a cavity will occur if the structure has certain dimensions, e.g., see Ref. 18. In particular, it is known that for TM polarization in an open circular dielectric resonator of radius a, which is filled with a material whose wave number is k, the first resonance is expected at $ka = 1.8412$ [20]. In the present case, the resonances occur at $k_2\rho_2 = 2.244$ for the DPS-DPS structure, and for the DPS-DNG structure at $k_2\rho_2 = 2.619$. Thus, the values of $k_2\rho_2$ for the open DPS-DNG and DPS-DPS structures are very close to the value associated with the natural resonance of the corresponding open circular dielectric resonator.

6. SUMMARY

In summary, significant enhancements of the total radiated and scattered powers, as compared with the power radiated by the source in free space, as well as the total scattering cross section, as compared to results obtained for the corresponding cylinder coated with a conventional material, were found by using specifically designed electrically small DPS-DNG structures. The benefits were associated with the so-called interface-resonance phenomena that may occur in such small structures [8]. The enhancements, which are found for a majority of the ELS locations, are considerably larger when the ELS is located near the interfaces of the layers where it can directly drive these interface resonances. Both dipolar and quadrupolar resonant structures were designed. The enhancements for the quadrupolar structures were significantly larger than those for the dipolar ones, but the resonances are proportionally narrower. Dispersion in the MTM coating was shown to narrow the resonances significantly in frequency, while

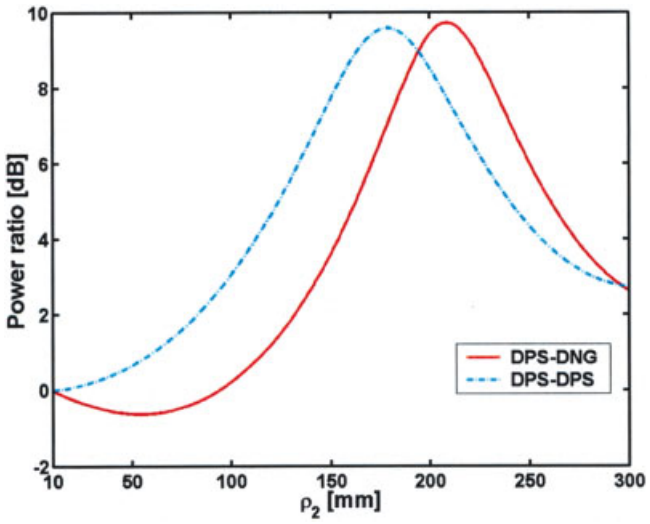

Figure 8 PR as a function of the outer shell radius ρ_2 for the DPS-DNG and DPS-DPS cylindrical structures when wavelength-sized natural resonances are expected. [Color figure can be viewed in the online issue, which is available at www.interscience.wiley.com]

the losses included in the dispersion models decreased the peak value of those resonances. It is worth remarking that it was shown that the present electrically small DPS-DNG structures, in contrast to the corresponding DPS-DPS structures, possess features that are similar to those associated with an electrically large radiator or scatterer. When the size of the MTM-coated cylinder was large enough for the wavelength-sized natural resonances to occur, it was shown that both the DPS-DNG and DPS-DPS structures had similar resonant enhancements of the total power, even for the ELS being located on the axis of the cylinders.

Other interesting applications of the present electrically small MTM structures, such as the possibility of reshaping the directivity and possibilities for obtaining directive electrically small antennas, have been considered. The results of these investigations will be presented elsewhere in the near future.

ACKNOWLEDGMENT

This work was supported in part by DARPA contract number HR0011–05-C-0068.

REFERENCES

1. V.G. Veselago, The electrodynamics of substances with simultaneously negative values of ε and μ, Sov Phys Usp 10 (1968), 509–514.
2. N. Engheta and R.W. Ziolkowski, A positive future for double negative metamaterials, IEEE Microwave Theory Tech 53 (2005), 1535–1556.
3. J.B. Pendry, Negative refraction makes a perfect lens, Phys Rev Lett 85 (2000), 3966–3969.
4. A. Alú and N. Engheta, Pairing an ε-negative slab with a μ-negative slab: Resonance, tunneling, and transparency, IEEE Trans Antennas Propag 51 (2003), 2558–2571.
5. V. Kuzmiak and A.A. Maradudin, Scattering properties of a cylinder fabricated from a left-handed material, Phys Rev B 66 (2002), 1161–1167.
6. R. Ruppin, Surface polaritons and extinction properties of a left-handed cylinder, J Phys Condens Matter 16 (2004), 5991–5998.
7. Ma.M. Khodier, Radiation characteristics of an infinite line source surrounded by concentric shells of metamaterials, In: IEEE antennas and propagation society symposium, Monterey, CA, 20–26 June, 2004.
8. A. Alú and N. Engheta, Resonances in sub-wavelength cylindrical structures made of pairs of double-negative and double-positive or ε-negative and μ-negative coaxial shells, In: Proceedings of the international electromagnetics in advanced applications conference, Turin, Italy, 8–12 September, 2003, pp 435–438.
9. A. Alú and N. Engheta, Polarizabilities and effective parameters for collections of spherical nano-particles formed by pairs of concentric double-negative (DNG), single-negative (SNG) and/or double-positive (DPS) metamaterial layers, J Appl Phys 97 (2005), 094310.
10. R.W. Ziolkowski and A. Kipple, Reciprocity between the effects of resonant scattering and enhanced radiated power by electrically small antennas in the presence of nested metamaterials shells, Phys Rev E 72 (2005), 036602.
11. C. Li and Z. Shen, Electromagnetic scattering by a conducting cylinder coated with metamaterials, In: Proceedings of the progress in electromagnetic research society meeting, PIERS'03, Honolulu, Hawaii, 2003, pp 91–105.
12. J. Sun, W. Sun, T. Jiang, and Y. Feng, Directive electromagnetic radiation of a line source scattered by a conducting cylinder coated with left-handed material, Microwave Opt Technol Lett 47 (2005), 274–279.
13. S.R. Nelatury, Comparing double-negative and double-positive covers around a radiating line current, Microwave Opt Technol Lett 48 (2006), 250–252.
14. R. Ruppin, Extinction properties of a sphere with negative permittivity and permeability, Solid State Commun 116 (2000), 411–415.
15. Z. Liu, Z. Lin, and S.T. Chui, Electromagnetic scattering by spherical negative-refractive-index particles: Low frequency resonance and localization parameters, Phys Rev E 69 (2004), 016619.
16. R.W. Ziolkowski and A. Kipple, Application of double negative metamaterials to increase the power radiated by electrically small antennas, IEEE Trans Antennas Propag 51 (2003), 2626–2640.
17. R.W. Ziolkowski and A. Erentok, Metamaterial-based efficient electrically small antennas, IEEE Trans Antennas Propag, submitted.
18. R.W. Ziolkowski and A. Erentok, At and beyond the Chu limit: Passive and active broad bandwidth metamaterial-based efficient electrically small antennas, IEEE Proc, submitted.
19. S.A. Tretyakov, S.I. Maslovski, A.A. Sochava, and C.R. Simovski, The influence of complex material coverings on the quality factor of simple radiating systems, IEEE Trans Antennas Propag 53 (2005), 965–970.
20. C.A. Balanis, Advanced engineering electromagnetics, Wiley, New York, 1989, Chap. 11.
21. M. Abramowitz and I.A. Stegun, Handbook of mathematical functions, Dover, New York, 1965, Chap. 10.

© 2006 Wiley Periodicals, Inc.

DESIGN OF BROADBAND TRANSPOLARIZING SURFACES

Pere J. Ferrer,[1] Brénam Kelem,[2] and Christophe Craeye[3]
[1] Grup d'Enginyeria Electromagnètica i Fotònica - TSC
Universitat Politècnica de Catalunya (UPC)
08034 Barcelona, Spain
[2] Département de Microélectronique et Télécommunications
Polytech' Marseille
13451 Marseille Cedex 20, France
[3] Laboratoire TELE
Université Catholique de Louvain (UCL)
1348 Louvain-la-Neuve, Belgium

Received 15 June 2006

ABSTRACT: *A transpolarizing reflector is proposed. It consists of periodic patches above a ground plane, with wide diagonal slots. For normal incidence, linear polarization along a principal direction is transformed into the orthogonal polarization with a 20-dB ratio over a 29.7% bandwidth. We prove that, in view of the diagonal symmetry of the structure, reflected fields in the principal directions must be in quadrature. The transpolarization bandwidth slowly decreases for incidence away from broadside. This surface very efficiently produces polarization conversion for circularly polarized incident fields. The quality of this conversion, described in terms of axial ratio, is obtained from the transpolarization level achieved in the linear polarization case.* © 2006 Wiley Periodicals, Inc. Microwave Opt Technol Lett 48: 2606–2611, 2006; Published online in Wiley InterScience (www.interscience.wiley.com). DOI 10.1002/mop.21989

Key words: *artificial magnetic conductor; transpolarization; reflecting surfaces; polarizers; linear and circular polarization*

1. INTRODUCTION

Transpolarizing surfaces may be used to reduce the reflectivity of scatterers, while offering polarization conversions. They may be considered for stealth applications, or for communication purposes, for which circular polarization [1], instead of linear, may be very useful.

Despite the intensive research carried out by different groups on reflectarrays [2, 3], deliberately transpolarizing reflectors have received very little attention in the literature. Two papers [4, 5] show surfaces designed for transformation from linear to circular polarization. The first considers, as we will do, high-impedance surfaces as a starting point, but the transpolarization level is relatively weak. The second reference shows a stronger conversion